Available online at www.sciencedirect.com
ScienceDirect
Journal of Nuclear Materials 373 (2008) 130–136
journal of nuclear materials
www.elsevier.com/locate/jnucmat

Effect of fast neutron fluence on the creep anisotropy of Zr–2.5Nb tubes

R.A. Holt [a,*], G.A. Bickel [b], N. Christodoulou [b,1]

[a] Queen's University, Kingston, Ontario, Canada
[b] Atomic Energy of Canada Ltd., Chalk River Laboratories, Chalk River, Ontario, Canada

Received 27 June 2006; accepted 8 May 2007

Abstract

The in-reactor behaviour of internally pressurised capsules of Zr–2.5Nb tubes is analysed in detail to separate the stress dependent component of deformation (creep). It is found by a rigorous statistical analysis that the creep rate varies with fast neutron fluence. At 555 K the axial creep rate increases while the transverse creep rate decreases with fluence. At 588 K the creep rate in both the axial and transverse directions increases with fluence. It is also shown that the creep anisotropy ratio R, i.e., the ratio of axial to transverse creep rate for a pressurised tube, varies with fluence, stress and irradiation temperature. These findings are discussed in terms of the irradiation-induced evolution in microstructure. The possible impact of the evolution of the dislocation substructure is discussed with reference to a self-consistent polycrystalline model that takes into account the crystallographic texture and the grain interaction strains present in zirconium alloys. The lower temperature creep behaviour is consistent with an increase with fast fluence of the single crystal creep compliance related to prismatic dislocation climb and glide, or a decrease in the single crystal creep compliances relating to basal and pyramidal slip. The creep behaviour at the higher irradiation temperature is more complicated, and there may be an influence of phase changes as well as dislocation structure. It appears that all three eigenvalues describing the single crystal creep behaviour depend on fast fluence.

1. Introduction

The anisotropic deformation of Zr–2.5Nb pressure tubes (PTs) during service in CANDU reactors [1–3] is related to the anisotropic physical properties of the hexagonal crystal structure of zirconium and the strong crystallographic texture developed during the manufacturing process [4]. The anisotropic properties of the single crystal also contribute to the development of a complex dislocation structure [5], grain morphology and second phase distribution [4]. The in-reactor deformation of zirconium alloys is due to irradiation growth, i.e., a shape change observed under no externally applied load, and creep, both thermal and irradiation induced. The resulting strain tensor is anisotropic [3,6,7].

Several studies have attempted to relate the anisotropic deformation of the polycrystalline zirconium alloys to those of individual grains by accounting for the microstructural features, particularly the crystallographic texture [3,6–11]. The development of these models depended on the availability of experimental data from creep tests on materials with properties similar to those exhibited by PTs. Since there are no direct tests that can readily be conducted on specimens obtained from full size PT to determine the anisotropic behaviour, small tubes were produced with properties similar to those of full size PTs and irradiated in the Osiris reactor in France [12,13]. In the most recent analysis of these experiments, we treated the creep anisotropy as independent of fast neutron fluence and temperature [7,11].

Subsequent microstructural studies have shown the densities of both **a**-type and **c**-component dislocations vary with neutron fluence, and that the functional dependencies of these variations on fluence, flux and temperature are different [14–18]. As well, the edge character **c**-component

* Corresponding author.
E-mail address: holt@me.queensu.ca (R.A. Holt).
[1] Now at the Canadian Nuclear Safety Commission, Ottawa, Ontario, Canada.

0022-3115/$ - see front matter
doi:10.1016/j.jnucmat.2007.05.033

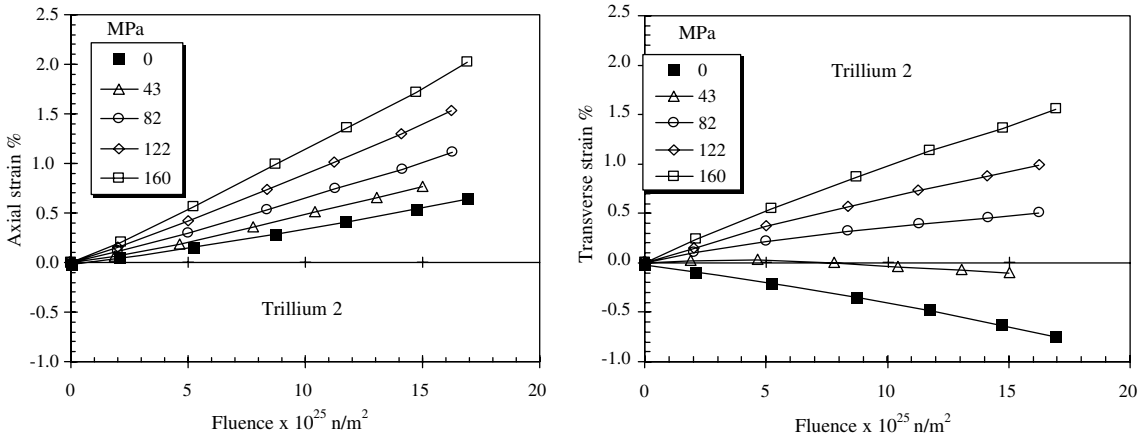

Fig. 1. Axial and transverse strain as a function of fast neutron fluence in Trillium 2 (555 K).

dislocations, initially with a Burgers vector of $1/3\langle 11\bar{2}3\rangle$ may split into two partials with Burgers vector $1/6\langle 20\bar{2}3\rangle$ [14] and those with screw character nucleate loops [16] which are likely faulted with a Burgers vector of $1/6\langle 20\bar{2}3\rangle$ or 1/2[0001]. Crystals of different orientation contain different initial populations of dislocations [16,19]. Furthermore, the morphology and phase structure of the 'β_{Zr}'-phase, whose boundaries with the α-phase appear to be important point defect sinks [10], change continuously with time, again as a complex function of temperature and fast neutron flux [17]. Finally, radiation induces fine precipitation of β_{Nb} in the α-grains of Zr–2.5Nb [17], which might influence glide, or provide recombination sites for the radiation induced point defects. Since the irradiation creep rate is believed to be controlled by the flux of irradiation-induced point defects to the dislocations and boundaries, and the differentials in these fluxes, it is highly unlikely that either the anisotropy or the creep rates are independent of fast neutron fluence, or that the anisotropy is independent of temperature. In view of this, we have reanalysed the data (with the addition of additional data points at higher fluence) to look for fluence and temperature dependencies.

2. Analysis of experimental results

The axial and transverse creep rate of the Trillium 2 (~555 K) and Trillium 3 (~588 K) were evaluated for the small tubes designated as MPT in Refs. [12,13]. Five specimens were measured in each experiment. One of the five samples was unpressurised (e.g., growth specimens M03 and M04 in Refs. [12,13]). The remaining four specimens were under nominal applied transverse stresses ranging from 40 to 160 MPa and axial stresses from 20 to 80 MPa. The measured strains as a function of fast fluence (i.e., $E > 1$ MeV) are shown in Figs. 1 and 2.

To calculate the creep rate, the growth term must be subtracted from the total strain. As is evident from Figs. 1 and 2, the growth samples were measured at somewhat different accumulated fluence than the pressurised capsules and therefore the growth term must be estimated by interpolation. A spline was used to fit the growth data and then the interpolated growth value was subtracted from the total strain.

It is advantageous to find a continuous function that describes the dependence of creep strain on fluence because it provides an analytical solution for the creep rate (as a

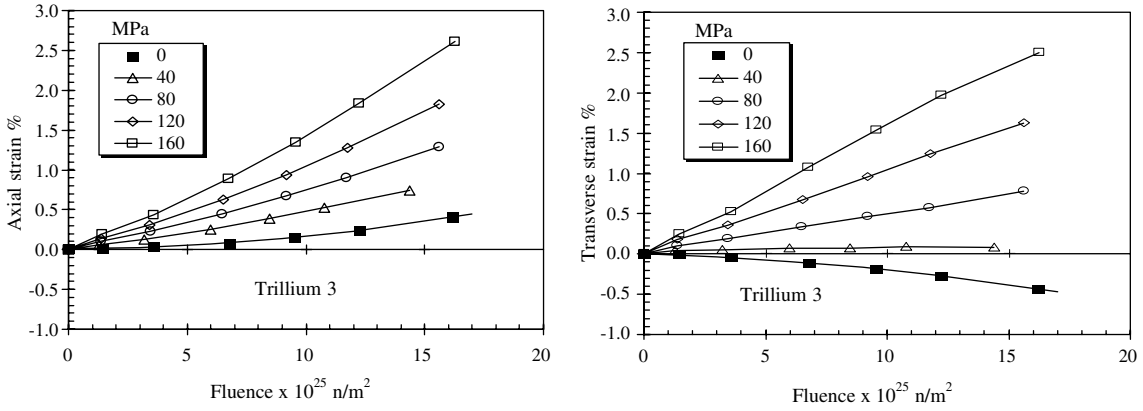

Fig. 2. Axial and transverse strain as a function of fast neutron fluence in Trillium 3 (588 K).

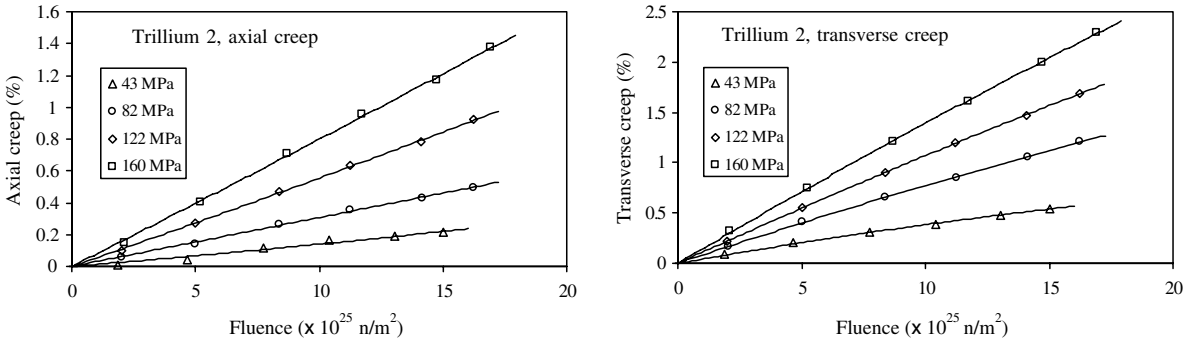

Fig. 3. Axial and transverse creep strain as a function of fast neutron fluence (after subtraction of interpolated growth) as a function in the Trillium 2 experiment (555 K).

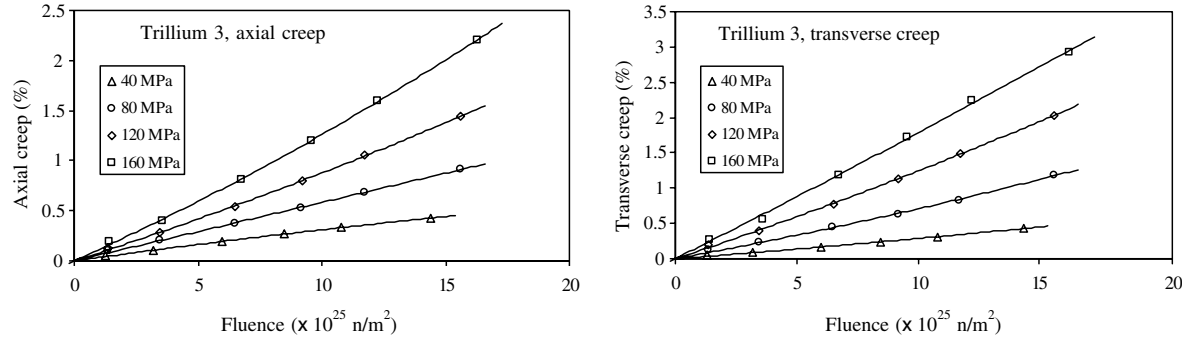

Fig. 4. Axial and transverse creep strain as a function of fast neutron fluence (after subtraction of interpolated growth) as a function in the Trillium 3 experiment (588 K).

function of fluence) and for the creep rate uncertainty. After the growth term has been subtracted (as described above), the creep strain was fitted to the polynomial function $\varepsilon^c = a_0\Phi + a_1\Phi^2$, where Φ is the accumulated fast fluence ($E > 1$ MeV). Good fits to this quadratic function were obtained (Figs. 3 and 4) and the fitting statistics are tabulated in Table A1 of Appendix A. The fitted function was then differentiated to provide the stain rate $d\varepsilon/d\Phi = a_0 + 2a_1\Phi$ with units '%/(10^{25} n/m^2, $E > 1$ MeV)'.

The strain rates and the associated uncertainties are shown as a function of fast neutron fluence in Fig. 5.

It is evident from Figs. 3–5 that the creep rate is not constant with fluence. At the lower temperature (i.e., Trillium 2 results) the axial rate appears to increase slightly with fluence (i.e., the creep rate is accelerating) whereas the transverse rate decreases with fluence (i.e., the creep rate is decelerating). In both directions the acceleration appears to be approximately independent of stress. The results are quite different at the higher temperature (i.e., Trillium 3 results). Except for the axial rate at 40 MPa, the axial and transverse rates increase with fluence. In particular, the acceleration of the axial rate increases with stress. In contrast to the lower temperature behaviour, the transverse rate accelerates with fluence, however at a lower value than that in the axial direction.

The ratio of the axial creep rate to the transverse creep rate, R, in a pressurised creep capsule (in which the axial stress is half the transverse stress) is a measure of the creep anisotropy. R can be calculated in a straightforward manner from the data in Table A1. The distribution function of R is calculated from a Monte Carlo sampling of the axial creep rate and transverse creep rate distributions[2]. The mean creep rate ratio R and the standard deviation are tabulated in Table A2 and are shown in Figs. 6 and 7. Note that the error bars only reflect the random scatter in the measurements. Systematic errors may be present that have not been taken into account.

From Figs. 6 and 7 it appears that the creep rate ratio R generally depends upon fluence, stress and temperature, varying between ~0.30 and 1.24 and in many cases the slope of R vs fast fluence is significant at the 95% confidence level. The mean value of R is 0.52 at 555 K and 0.81 at 588 K with an overall average of 0.67. The value of R reported in [12] was 0.715. At 555 K the creep rate ratio R appears to weakly increase with fluence for all applied stress levels, whereas at 588 K the ratio decreases

[2] Ten thousand 'data' pairs are randomly generated from two model normal distributions: one model distribution is described by the mean and standard deviation of the fitted axial strain (the numerator) and the other model distribution is described by the mean and standard deviation of the fitted transverse strain (the denominator). The results from the 10 000 pairwise ratios provide the distribution of ratios.

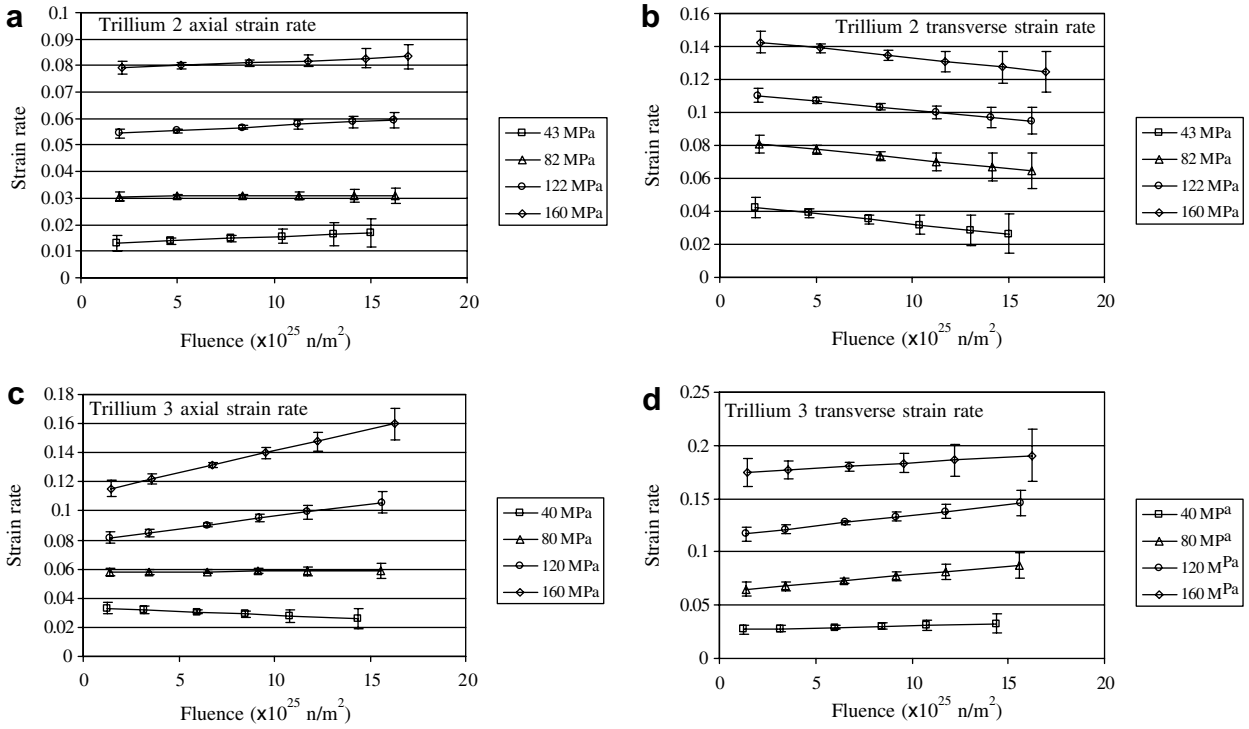

Fig. 5. Creep rate calculation and uncertainties (error bars are 2 standard deviations). The creep rate is in units of % strain per 10^{25} n/m^2, $E > 1$ MeV.

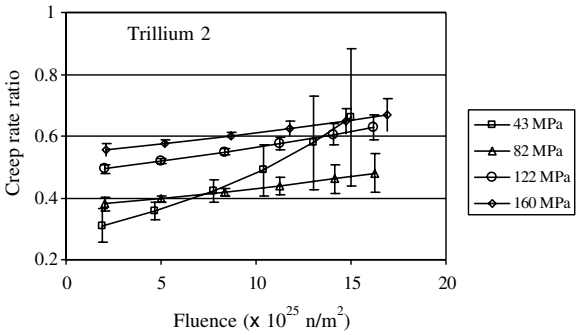

Fig. 6. Biaxial creep rate ratio R as a function of fluence in Trillium 2 (555 K). Error bars are uncertainties at the 2 standard deviation level.

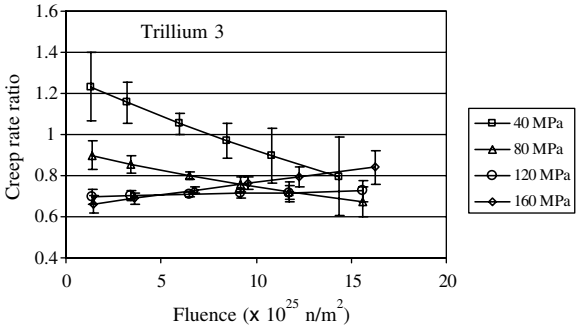

Fig. 7. Biaxial creep rate ratio R as a function of fluence in Trillium 3 (588 K). Error bars are uncertainties at the 2 standard deviation level.

with fluence at lower applied stresses while it increases slightly with fluence at higher applied stresses.

3. Discussion

Since the crystallographic texture and grain structure remain unchanged during irradiation at the temperatures of interest, it is reasonable to assume that the dependence of the creep rates and creep anisotropy on fluence should be related to the evolution of the β-phase and the dislocation structure and the precipitation of β_{Nb} in the α-phase.

Assessing the effects of the phase distribution and changes in the phase boundaries on the anisotropy of creep is impossible, since we have little information on these changes, and the deformation models do not, thus far consider these features. However, some insight into the effects of the dislocation substructure on the creep may be gained by examining the models that have been developed for the deformation. The necessity to provide such models to predict in-service performance has led to the assumption that long-term deformation consists of additive components from thermal creep, irradiation creep and irradiation growth [6–11]. These components are anisotropic and contribute to length as well as diameter changes. Christodoulou et al. [11] discussed the observed creep anisotropy of the internally pressurised capsules by means of an equation proposed earlier [7] that includes the three additive terms mentioned above. In [11] the creep anisotropy ratio for irradiation creep was determined by calculating the Hill's anisotropy constants F, G and H, and the creep anisotropy ratio R is proportional to $\frac{H-F}{2G+F}$. Here the axial and transverse creep rates are proportional to $(H - F)$ and $(2G + F)$ respectively.

The Hill's anisotropy constants were calculated by means of a self-consistent computer code SELFPOLY

[7,20] that takes into account the crystallographic texture and an assumed single crystal creep model. Based on the symmetry of the hcp crystal, the single crystal creep model assumes a creep compliance tensor with three independent eigenvalues k_1, k_2 and k_3. No particular creep mechanism is assumed, but if dislocation glide is the strain producing step (for the climb-assisted glide mechanism, for example) these three eigenvalues are associated primarily with pyramidal, prismatic and basal slip [7–9,11]. The set of eigenvalues k_1, k_2 and k_3 used by Christodoulou et al. [11] were derived in [7] and had equivalent values of 0.2, 5.0 and $2.0\times10^{-9}\,\mathrm{h^{-1}\,MPa^{-1}}$, respectively, for fast neutron flux of $1.96\times10^{17}\,\mathrm{n/m^2\,s^{-1}}$, $E>1$ MeV and a temperature of 555 K corresponding to the average conditions in an early commercial CANDU nuclear generating station. These scale with fast neutron flux (being equivalent to 0.28, 7.09 and $2.8\times10^{-3}\%\times(10^{25}\,\mathrm{n/m^2})^{-1}\times\mathrm{MPa^{-1}}$ in the units of strain rate used in this paper) and have the same temperature dependence as defined in [11]. The values of k_i were assumed to remain constant with fast neutron fluence and to be the same for all grains regardless of their orientation. These assumptions do not allow for any evolution of the creep anisotropy ratio with temperature and fluence or any dependence upon stress. An attempt to include an effect of the evolution of microstructure was made by Tomé and Christodoulou in [21], however many somewhat arbitrary assumptions were required, and no experimental evidence was presented to verify that the creep rates in fact changed with fast neutron fluence.

A qualitative interpretation of the dependence of creep rate on fluence and temperature can be inferred from a calculation of the axial and transverse creep rate and their ratio R by varying one single crystal creep compliance while keeping the other two values constant and equal to the values mentioned above. This is shown in Figs. 8(a)–(c), where it can clearly be seen that the transverse strain rate increases, the axial rate decreases and R decreases with increasing k_1. The transverse rate decreases, the axial rate increases and R increases with increasing k_2, and both the axial and transverse rates increase, while R decreases with increasing k_3.

The observed behaviour at 555 K where the transverse strain rate decreases, the axial strain rate increases and R increases with fast fluence could be explained by some combination of k_1 decreasing, k_2 increasing and/or k_3 decreasing with fast fluence. Microstructural observations [11–18] have shown that in the temperature range 520–570 K, the **a** dislocation density increases gradually with fluence by the formation of prismatic loops or remains constant (the gradual increase could be due to the **a** component of **c** + **a** dislocations). Thus k_2 would remain constant or increase slightly. The **c** + **a** dislocation density increases at a faster rate, however this increase in the **c** + **a** dislocation density is associated with observed splitting of pre-existing edge dislocations into partials rendering them sessile [14], and nucleation of faulted loops (also sessile) on screw dislocations [14,16], hence the density of mobile **c** + **a** dislocations likely decreases with fluence, and this would contribute mainly to a decrease in k_1.

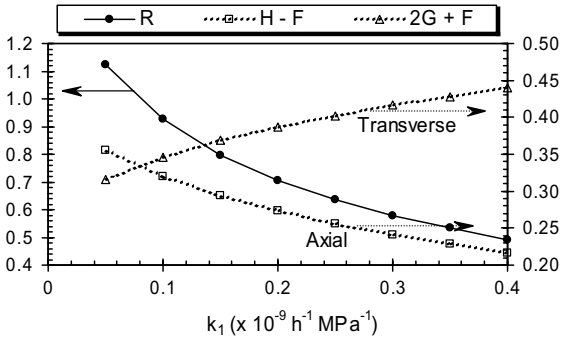

Fig. 8(a). Variation of $(H-F)$, $(2G+F)$ and R with single crystal creep compliance k_1.

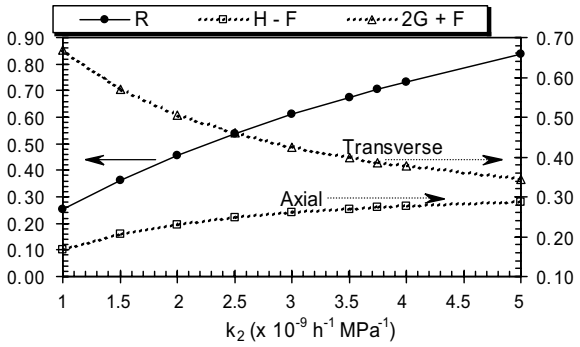

Fig. 8(b). Variation of $(H-F)$, $(2G+F)$ and R with single crystal creep compliance k_2.

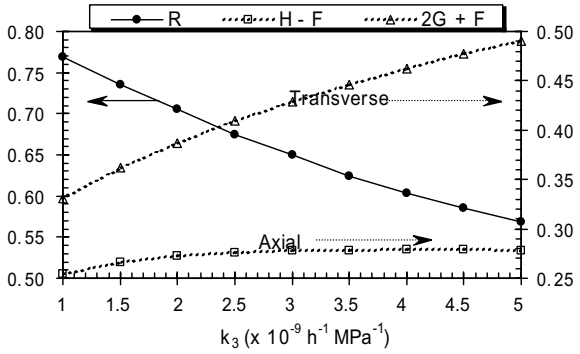

Fig. 8(c). Variation of $(H-F)$, $(2G+F)$ and R with single crystal creep compliance k_3.

The creep behaviour at 588 K is more complicated than at 555 K. It appears that more than one of the single crystal creep compliances must change, and by different amounts and perhaps in different directions at different stresses. This suggests an increased role of both stress and temperature in modifying the dislocation structure, and perhaps an influence of phase changes on the creep. However there are few data on the changes in dislocation structure that occur at this higher temperature.

Of course, it is also possible that phase or phase boundary changes are having an effect at both temperatures since

the phase boundaries are thought to be important point defect sinks [10]. This could certainly affect the irradiation growth behaviour, and might effect the absolute creep rate, but is thought unlikely to affect the creep anisotropy because the proportions of the different dislocations present and their movements are unlikely to be affected.

The awareness of this evolution of properties is important for the maintenance and life extension of existing CANDU reactors [22] as well as prediction of the performance of pressure tubes in advanced CANDU reactors [23] that will operate at conditions more extreme than those of current designs. Of particular interest is the few millimeters of sag of the pressure tubes between the fuel channel spacers which can limit their life if they contact the cold calandria tube that is nominally concentric with the pressure tube [24]. Sag is the response to the bending moment induced by the weight of fuel and coolant in the tube, effectively a uniaxial loading condition in the length direction of the tube, a condition totally different from the biaxial stress tensor imposed by pressurisation. The measured sag of several tens of millimeters actually reflects the sag properties of the cool calandria tube. The only way to assess the sag properties of the pressure tube per se is the use of models representing the anisotropy. It is therefore extremely important that this be understood, and that changes occurring as a result of service be taken into account.

4. Conclusions

The in-reactor behaviour reported earlier for internally pressurised capsules of Zr–2.5Nb at 555 and 588 K has been analysed in more detail by carrying out a rigorous statistical analysis. It was found that the creep rate and creep anisotropy both vary with fast neutron fluence and temperature. At 555 K, the axial creep rate increases while the transverse creep rate decreases with fluence, resulting in an increase in the anisotropy ratio R at all stresses. At 588 K the creep rate in both the axial and transverse directions increases with fluence, but the changes in the anisotropy ratio vary with stress. The findings are discussed with respect to observed microstructural changes, and with reference to a polycrystalline model developed to predict in-service deformation behaviour of Zr–2.5Nb tubes. A plausible explanation for the behaviour at 555 K is developed, relating to changes in the dislocation structure. However, the lack of microstructural data for irradiation at the higher temperature render any statements about the causes of the changes in creep behaviour with fast fluence and stress speculative.

Acknowledgments

One of the authors (R.A.H.) thanks the Natural Sciences and Engineering Research Council of Canada, Ontario Power Generation, the CANDU Owners Group and Nu-Tech Precision Metals for financial support under the Nuclear Materials Chair program at Queen's University.

Appendix A

See Tables A1 and A2.

Table A1
Statistics for strain rates fitted as a function of fluence

Stress (MPa)	a_0	sd(a_0)	A_1	sd(a_1)	s^2	R^2
Trillium 2: axial						
43	0.0125	0.0014	1.5×10^{-4}	1.1×10^{-4}	6.1×10^{-5}	0.99664
82	0.03062	0.00076	8.0×10^{-6}	5.5×10^{-5}	2.1×10^{-5}	0.99979
122	0.05367	0.00077	1.8×10^{-4}	5.6×10^{-5}	2.1×10^{-5}	0.99993
160	0.0785	0.0012	1.43×10^{-4}	8.5×10^{-5}	5.9×10^{-5}	0.99992
Trillium 2: transverse						
43	0.0445	0.0031	-6.1×10^{-4}	2.4×10^{-4}	2.9×10^{-4}	0.99758
82	0.0831	0.0028	-5.7×10^{-4}	2.0×10^{-4}	2.9×10^{-4}	0.99952
122	0.1125	0.0021	-5.5×10^{-4}	1.5×10^{-4}	1.5×10^{-4}	0.99986
160	0.1451	0.0032	-6.0×10^{-4}	2.2×10^{-4}	4.0×10^{-4}	0.99981
Trillium 3: axial						
40	0.0339	0.0016	-2.8×10^{-4}	1.4×10^{-4}	8.4×10^{-5}	0.99862
80	0.0581	0.0013	2.3×10^{-5}	9.7×10^{-5}	5.8×10^{-5}	0.99978
120	0.0793	0.0018	8.5×10^{-4}	1.4×10^{-4}	1.2×10^{-4}	0.99981
160	0.1112	0.0026	1.5×10^{-3}	1.9×10^{-4}	2.7×10^{-4}	0.99981
Trillium 3: transverse						
40	0.0265	0.0021	2.1×10^{-4}	1.8×10^{-4}	1.4×10^{-4}	0.99743
80	0.0627	0.0030	8.0×10^{-4}	2.3×10^{-4}	3.2×10^{-4}	0.99921
120	0.1141	0.0028	1.02×10^{-3}	2.2×10^{-4}	2.9×10^{-4}	0.99977
160	0.1729	0.0060	5.5×10^{-4}	4.5×10^{-4}	1.4×10^{-3}	0.99948

Table A2
Ratio of axial to transverse creep rate from the Trillium 2 and 3 experiments

Stress (MPa)	Fluence[a]	R[b]	2sd[c]	Stress (MPa)	Fluence[a]	Ratio[b]	2sd[c]
Trillium 2							
43	1.88	0.311	0.055	122	2.01	0.493	0.015
	4.65	0.357	0.029		5.00	0.518	0.008
	7.77	0.422	0.035		8.37	0.549	0.009
	10.40	0.490	0.082		11.23	0.576	0.019
	13.06	0.578	0.153		14.10	0.606	0.033
	15.01	0.660	0.222		16.22	0.629	0.041
82	2.02	0.380	0.023	160	2.01	0.555	0.021
	5.00	0.396	0.011		5.00	0.576	0.010
	8.37	0.418	0.012		8.37	0.602	0.011
	11.27	0.439	0.027		11.23	0.625	0.024
	14.14	0.461	0.045		14.10	0.650	0.040
	16.26	0.480	0.062		16.22	0.669	0.052
Trillium 3							
40	1.28	1.233	0.168	120	1.37	0.699	0.035
	3.20	1.156	0.101		3.43	0.703	0.022
	5.98	1.052	0.049		6.51	0.709	0.011
	8.47	0.970	0.086		9.20	0.714	0.021
	10.79	0.897	0.132		11.75	0.718	0.034
	14.37	0.796	0.193		15.62	0.725	0.051
80	1.37	0.899	0.069	160	1.43	0.663	0.042
	3.44	0.856	0.040		3.58	0.690	0.027
	6.48	0.800	0.019		6.76	0.729	0.015
	9.17	0.758	0.034		9.56	0.763	0.029
	11.72	0.721	0.051		12.23	0.794	0.050
	15.59	0.673	0.074		16.26	0.840	0.080

[a] Fluence in units of 10^{25} nm^{-2}.
[b] R = axial creep rate divided by transverse creep rate.
[c] 2sd ~ 2 standard deviations on the value of R.

References

[1] R.A. Holt, A.R. Causey, V. Fidleris, Dimensional Stability and Mechanical Behaviour of Irradiated Metals and Alloys, vol. 1, British Nuclear Energy Society, London, 1983, p. 175.
[2] V. Fidleris, J. Nucl. Mater. 159 (1988) 22.
[3] A.R. Causey, R.A. Holt, S.R. MacEwen, in: D.G. Franklin, R.B. Adamson (Eds.), Zirconium in the Nuclear Industry: 6th International Symposium, ASTM-STP-824, American Society for Testing of Materials, Philadelphia, 1984, p. 269.
[4] B.A. Cheadle, in: Proceedings of the 3rd International Symposium on Zirconium in the Nuclear Industry, ASTM STP 633, 1977, p. 457.
[5] R.A. Holt, M. Griffiths, R.W. Gilbert, J. Nucl. Mater. 149 (1987) 51.
[6] R.A. Holt, E.F. Ibrahim, Acta Metall. 27 (1979) 1319.
[7] N. Christodoulou, A.R. Causey, C.H. Woo, C.N. Tomé, R.J. Klassen, R.A. Holt, in: A.S. Kumar, D.S. Gelles, R.K. Nanstad, E.A. Little (Eds.), Effects of Radiation on Materials: 16th International Symposium, ASTM-STP-1175, American Society for Testing of Materials, Philadelphia, 1993, p. 1111.
[8] C.H. Woo, J. Nucl. Mater. 150 (1985) 105.
[9] C.H. Woo, in: Proceedings, British Nuclear Society, London, 1987, p. 65.
[10] R.A. Holt, J. Nucl. Mater. 159 (1988) 310.
[11] N. Christodoulou, A.R. Causey, R.A. Holt, C.N. Tomé, N. Badie, R.J. Klassen, R. Sauvé, C.H. Woo, in: E.R. Bradley, G.P Sabol (Eds.), Zirconium in the Nuclear Industry: 11th International Symposium, ASTM-STP-1295, American Society for Testing of Materials, West Conshohocken, 1996, p. 518.
[12] R.G. Fleck, J.E. Elder, A.R. Causey, R.A. Holt, in: Proceedings of the 10th International Symposium on Zirconium in the Nuclear Industry, ASTM-STP 1245, 1994, p. 168.
[13] A.R. Causey, R.A. Holt, N. Christodoulou, E.T.C. Ho, in: G.P. Sabol, G.D. Moan (Eds.), Zirconium in the Nuclear Industry: 12th International Symposium, ASTM-STP-1354, American Society for Testing of Materials, West Conshohocken, PA, 2000, p. 74.
[14] P.H. Davies, R.R. Hosbons, M. Griffiths, C.K. Chow, in: Proceedings of the 10th International Symposium on Zirconium in the Nuclear Industry, ASTM-STP 1245, 1994, p. 135.
[15] M. Griffiths, J.F. Mecke, J.E. Winegar, in: E.R. Bradley, G.P Sabol (Eds.), Proceedings of the 11th International Symposium on Zirconium in the Nuclear Industry, ASTM-STP-1295, American Society for Testing of Materials, West Conshohocken, 1996, p. 580.
[16] R.A. Holt, A.R. Causey, M. Griffiths, E.T.C. Ho, in: Proceedings of the 12th International Symposium on Zirconium in the Nuclear Industry, ASTM-STP 1354, 2000, p. 86.
[17] V.F. Urbanic, M. Griffiths, in: Proceedings of the 12th International Symposium on Zirconium in the Nuclear Industry, ASTM-STP 1354, 2000, p. 641.
[18] M. Griffiths, P.H. Davies, W.G. Davies, S. Sagat, in: Proceedings of the 13th International Symposium on Zirconium in the Nuclear Industry, ASTM-STP 1423, 2002, p. 507.
[19] M. Griffiths, R.A. Holt, J. Li, S. Saimoto, Microstructural Science, vol. 26, ASM International, Materials Park, 1999, p. 293.
[20] C.N. Tomé, C.B. So, C.H. Woo, Philos. Mag. A 67 (1993) 917.
[21] C.N. Tomé, N. Christodoulou, Philos. Mag. A 80 (2000) 1407.
[22] R.A. Holt, H. Wong, Nucl. Energy 40 (2002) 69.
[23] J. Hopwood, in: Proceedings of the 26th Annual Conference of the Canadian Nuclear Society, Paper P23, 2005.
[24] R.A. Holt, J. Nucl. Mater., in press, doi:10.1016/j.jnucmat.2007.02.017.